ISSN 2504-9593
DOI: 10.5281/zenodo.20197274
https://ijree.com/index.php/publications/article/view/45
Int. J. Renew. Energ & Environ Vol.4 (2), pp 77-97(2026)

NANOCOMPOSITE MATERIAL OF CARBON NANODOTS-COPPER OXIDE (CNDs-CUO) FROM *RAPHIA HOOKERI SEED (RHS)* FOR INVESTIGATION OF ELECTROCHEMICAL ENERGY STORAGE

[1,2]Akpeji, B.H., [3]Iyasele, J.U., [2,4]Elemike, E.E., [1] Okhuarobo, L.O., [5]Akpeji, S.A.

[1]Department of Science Laboratory Technology, Federal University of Petroleum Resources, Effurun, Delta State
[2]Centre for sustainable development goal, Federal University of Petroleum Resources, Effurun, Delta State, Nigeria.
[3]Department of Chemistry, University of Benin, Benn City, Edo State.
[4]Department of Chemistry, Federal University of Petroleum Resources, Effurun, Delta State
[5]Centre for Information and Communication Technology, Federal University of Petroleum Resources, Effurun, Delta State.
Corresponding author's Address: akpeji.honesty@fupre.edu.ng. +2348060174341

Abstract

The present work is aimed at exploring the synthesis and electrochemical capabilities of carbon nanodot-copper oxide (CND-CuO) nanocomposites prepared from Raphia hookeri seed biomass. Through hydrothermal carbonization, CNDs were prepared whereas CuO NPs were made solvothermally with RHS extract, acting as a reducing agent. Formation of composite was carried out by hydrothermal process. Phytochemical assays were known to be flavonoid, phenols, tannin, saponins, alkaloid, terpenoids, glycosides, and reducing sugars. The UV Vis spectra revealed the absorption maxima at 280 nm (CNDs), 301 nm (CuO) and at 288 nm (CND Cu O), which is an indication of the electronic interaction. Band gaps were 2.40, 2.29, and 2.32 eV. TEM disclosed the size of particles of 6.35, 21.0, and 14.2 nm whereas SEM depicted porous CuO and consistent composite micro morphology. OH, C=O, C-O and CuO groups were detected by FTIR, which confirmed the formation of composites. EDX analysis indicated Cu (54.66%), C (40.34%), and O (5.00%). Electrochemical impedance spectroscopy displayed increased redox peaks and capacitance and cyclic voltammetry indicated decreased resistance to charge transfer. The stability of CuO was verified by thermogravimetric analysis. The CND-CuO nanocomposite exhibited electrochemical functionality, indicating that it could potentially be utilized across a wide range of energy storage applications.

Keywords: Copper oxide nanoparticles (CuO-NPs), RHS, energy storage, synthesis, characterization, electrochemical.

1.0 INTRODUCTION

The world has increased the call to adopting sustainable energy systems that have increased the need to develop high performance energy storage. The traditional energy storage media, especially batteries and supercapacitors, can typically be constrained by trade-offs between energy density and power density and long-term cycling life (Sead *et al*., 2025; Ren *et al*., 2026). Recently, studies in this area have also started to give a strong emphasis on nanostructured materials, particularly carbon-based nanomaterials, owing to its wonderful physicochemical characteristics (Zhang *et al*., 2020; Surana *et al.,* 2025). CNDs are one of these promising nanomaterials that are classified as zero-dimensional nanomaterials with high surface area, controlled surface functionalities, and good electrical conductivity as well as excellent electrochemical stability (Sikiru *et al*., 2023; Sohouli *et al.,* 2023;

Mohammed *et al.,* 2025). These properties allow faster charge dynamics, faster diffusion of ions, and more active redox reaction sites, which allows CNDs to be very effective in energy storage systems of the future (Jin, 2024; Mohammed *et al.,* 2025; Huang et al., 2025; Chakrabarti *et al.,* 2025). It is also important to note that recent developments show that, by embellishing dots with heteroatoms, one can enhance such parameters as capacitance, rate capacity, and cycling stability of supercapacitors and battery systems by orders of magnitude as compared to traditional electrode materials (Sead *et al.,* 2025; Haghjou *et al.,* 2025; Gusain *et al.,* 2025). Simultaneously, the combination of transition metal oxides with carbon dots has been subjected to significant attention as a method of addressing the inherent drawbacks of either of the constituents. Oxides of transition metals like copper oxide (CuO) are highly theoretical and have high redox activity but poor electrical conductivity and structural instability in charge discharge cycles limit their practical use. It has been shown in recent studies that, when carbon dots are incorporated into metal oxide matrices, the nanocomposites obtained exhibit synergy and enhanced electrochemical performance (Zhang *et al.,* 2023; Leta *et al.,* 2025; Tavan *et al.,* 2025; Mametja *et al.,* 2026). Carbon dots serve as efficient conduction channels, enhance electron transport cycle, inhibit recombination, and more active sites to trigger electrochemical reactions, which results in a considerable increase in energy storage efficiency (Zhao *et al.,* 2021; Arora *et al.,* 2024; Mohammed *et al.,* 2025; Mametja *et al.,* 2026). Moreover, nanocomposites of CNDSs to metal oxides have demonstrated higher specific capacitance, quicker charge discharge capacities and better cycling endurance which has placed them in the view as going to power next generation supercapacitor and hybrid energy storage. Important new aspect in the field is the utilization of biomass precursors to produce carbon-based nanomaterials, in line with the global sustainability and circular economy objectives. Farm wastes and plant materials that are underused or underutilized like RHSs are renewable, low-cost feedstocks of carbon time-rich green syntheses of carbon dots. Biomass-modified CNDSs (in addition to decreasing environmental load) bring about intrinsic heteroatoms and functional groups which yield enhanced electrochemical performance. Recent research emphasizes that these green-synthesized CNDSs have similar or better advantage against their chemically-synthesized counterparts, especially in energy storage (Akpeji *et al.,* 2024; Surana, 2025; Sikiru *et al.,* 2023; Mohammed *et al*., 2025; Ren *et al*., 2026). Nevertheless, in spite of such developments, little work has been done on the elaboration of CNDS-CuO nanocomposites that are particularly based on RHS biomass especially when it comes to the evaluation of energy storage performance. This loophole highlights the novelty of the current work (that aims to investigate a sustainable, cost-effective, and high-performance nanocomposite-based system in order to be used in the process of energy storage), thus, not only playing a role in materials innovation but also in environmental sustainability.

2.0 MATERIALS AND METHODS

2.1 Materials

Fresh seeds of *Raphia hookeri* were collected, authenticated, and appropriately processed for subsequent analysis. All reagents employed were of quality grade and included distilled

water, copper acetate dihydrate [$Cu(CH_3COO)_2.2H_2O$], ethanol (C_2H_5OH), methanol (CH_3OH), hydrochloric acid (HCl), sulfuric acid (H_2SO_4), acetic anhydride, ferric chloride ($FeCl_3$), Mayer's reagent, Wagner's reagent, Dragendorff's reagent, Benedict's reagent, Fehling's solutions A and B, ammonia solution, sodium hydroxide (NaOH), chloroform, lead acetate, and other standard laboratory chemicals.

2.2 Method

2.2.1 Preparation of aqueous extract

The seeds of Raphia hookeri were gathered at Ukwani Local Government Area, Delta State, Nigeria, and later authenticated at the Department of Plant Biology and Biotechnology, University of Benin. Before the extraction, the kind of seeds harvested were washed, dried in air and ground into a fine powder. To extract the aqueous extract of RHS, the Soxhlet method of extraction was used, according to (Akpeji and Singh, 2026; and Okewale and Akpeji, 2022) methods. In short 100 g of powdered RHS sample was weigh in into a cellulose thimble and loaded into a Soxhlet extractor which was hooked up to a round-bottom flask filled with distilled water as extracting solvent. This apparatus was placed in a heating mantle and the solvent was heated to its boiling point and then was allowed to vaporize, condense via the condenser and flow through the sample matrix repeatedly. The extraction process was upheld over a period of about four hours and constant siphoning was done to ensure effective harvest of phytochemical constituents. Exhaustive extraction was referred to when the thimble with the solvent was clear indicating that all the extractable compounds were accumulated. During the process, the condenser temperature was extremely controlled at a low level to promote the efficiency of condensation and maximum solvent recovery. After the extraction, aqueous extract was harvested and concentrated through controlled heating at 80 long degrees in order to minimize the volume of the solvent. This action helped in part water removal and produced a more concentrated extract. The extract was further refined to get refined aqueous extract that can be used in further phytochemical screenings and experimentations.

2.2.2 Qualitative Phytochemical Screening

The aqueous extract of RHS was also analyzed qualitatively to identify the presence of important phytochemical constituents through routine practice as described by Akpeji *et al.* 2026), with a few modifications.

2.2.2.1 Alkaloids Test

The extract was acidified with dilute hydrochloric acid and an aliquot of the extract was filtered. The resultant filtrate was separated and subjected to Mayer, Wagner and Dragendorff reagents independently. The presence of the alkaloids was confirmed by the appearance of the cream, reddish brown or orange precipitates respectively.

2.2.2.2 Flavonoids Test (Shinoda Method)

Small fragments of magnesium were added to the extract, and a very little concentrated hydrochloric acid was slowly added to it. The outbreak of pink color to red color suggested flavonoids.

2.2.2.3 Tannins Test

One part of the extract was reacted with the 1% solution of ferric chloride. A blue-black or green colouration was evidenced to be a result of tannins.

2.2.2.4 Saponins Test (Foam Test)

Extract pure was mixed with distilled water and stirred up. The existence of foam that was formed and lasted a few minutes was a sign of the existence of saponins.

2.2.2.5 Phenols Test

A few drops of ferric chloride solution were added to the extract. The development of a deep blue or black coloring was an indicator of phenolic compounds.

2.2.2.6 Glycosides Test (Keller–Killiani Reaction)

The extract was mixed with glacial acetic acid with a trace of ferric chloride with caution and, subsequently, concentrated sulfuric acid was added to the edge of the test tube. The interface was also surrounded by a brown colorant that showed that it contained cardiac glycosides.

2.2.2.7 Reducing Sugars Test (Benedicts Method)

Extract was put into a testube in a water bath with Benedict reagent and allowed to heat. It was confirmed that reducing sugars were produced by developing green, yellow or brick-red precipitate.

2.2.2.8 Reducing Sugars Test (Method of Fehling)

An equal amount of the Fehling solutions A and B was prepared and taken directly to the extract and then heated. The fact that a brick-red precipitate was formed was indicative of the presence of reducing sugars.

2.2.2.9 Steroids Test (Salkowski Reaction)

Chloroform was added, and concentrated sulfuric acid was added in the extract can carefully. The presence of steroids was confirmed by a reddish-brown colouration.

2.2.2.10 Terpenoids Test

The extract was treated with chloroform and layered with concentrated sulfuric acid. The appearance of reddish-brown interface was a sign of terpenoids.

2.2.2.11 Anthraquinones Test (Method of Borntrager) The extract was boiled using dilute sulfuric acid, filtered and extracted using chloroform. When the chloroform layer was added ammonia solution, a pink or red-colour suggestive of anthraquinones, appeared.

2.2.3 Synthesis of CuO NPs

The seeds of the *Raphia hookeri* which were used in this synthesis were obtained in the cub and thoroughly washed with distilled water to remove impurities sticking to the seed. Air drying of the cleaned seeds was done in seven days and then they were milled into fine powder using a laboratory grinder. The 4 g amount of the powdered sample was weighed and transferred into a clean conical flask and it was mixed with 200ml of distilled water. The solution was left to heat on a heating mantle and allowed to heat the mixture to 2 hours to allow aqueous extraction and then filtered to get extract. Then 20 mL of aqueous extract of *RHS* was put in the 400 mL of 0.1 M copper acetate 1:10 (v/v) ratio. Then, 20 mL of the 1 M sodium hydroxide (NaOH) solution was added to the mixture. The formulation of the resulting solution was kept stirring at 80 ^{o}C with the help of a magnetic stirring to encourage the formation of nanoparticles. The process synthesis was followed up with the help of the UV-visible spectrophotometer to monitor the development of CuO NPs. The process was monitored until an absorbance peak 301 nm was attained and the specific absorption wavelength of CuO NPs was achieved according to the literature (Da'na *et al*., 2024). The overall time of reaction in nanoparticles formation was about 2 hours. A colour change was evident in the process, and the colour changed to blue then to a dark black colour of copper oxide, and on the other hand. This shift meant that the $Cu(OH)_2$ was formed and the further processing resulted in the production of CuO nanoparticles in varying

petri dishes. The precipitate thus obtained was centrifuged at 5000 rpm and dried in an LD-201-E drying oven (Vision Scientific) at 80 °C and calcined at 300 °C for 30 minutes. The general synthesis step is summarized in the following equation 1.

$$[Cu(CH_3COO)_2.2H_2O] + (metabolites\ from\ R.H.S) + 1M\ NaOH \rightarrow Cu(OH)_2 + drying\ to\ remove\ H_2O + calcination \rightarrow CuO - NPs$$

equation 1

2.2.4 Synthesis of functionalized CNDs from RHS

The CNDs was synthesized using procedures of (Akpeji *et al.,* 2024a; Akpeji *et al.,* 2024b; Okhorie and Akpeji, 2025; Akpeji *et al.,* 2025) with slight modification in temperature. RHS were collected from natural populations in Ukwani Local Government Area, Delta State, Nigeria. Botanical identification of the plant material was carried out by in the Department of Plant Biology and Biotechnology, University of Benin, Edo state, Nigeria. The seeds were thoroughly washed with distilled water to remove adhering impurities and air-dried at ambient laboratory temperature for ten (10) days to achieve constant weight. The dried seeds were subsequently pulverized into a fine powder using a laboratory-grade grinder to increase surface area and ensure uniform thermal treatment. 300 g of the powdered RHS was subjected to carbonization in a muffle furnace at 500 °C for 2 hours under controlled heating conditions. The carbonized material obtained was transferred into 2000 mL beaker with 500 mL distilled water under a heating mantle, positioned on overhead stirrer and maintained under continuous heating with constant agitation for 6 hours. During this stage, aliquot samples were periodically withdrawn and examined under a UV lamp to monitor photoluminescent behavior. The reaction was terminated once a stable green fluorescence was observed, indicating the formation of CNDs structures. Finally, the formed CNDs was activated with 0.05 M NaOH to increase functionalization and electrochemical performance. The product was allowed to dry in multiple Petri dishes at room temperature, after which the solid residue was gently scraped, collected into airtight sample containers, and preserved for subsequent physicochemical characterization and electrochemical performance evaluation.

2.2.5 Synthesis of CNDs-CuO nanocomposite

The synthesis of CNDs-CuO nanocomposite was done through hydrothermal technique with distilled water as the solvent. CNDs and CuO nanoparticles were accurately weighed (equimolar, 1:1) and dissolved individually in distilled water and swirled to dissolve the solids completely. The two nanofluids were then mixed in one reaction vessel and stirred with magnetic stirrer at 80 °C to enhance uniform mixing and allow bond interaction, to enable the nucleation and growth of the CNDs-CuO nanocomposite. The formation of the nanocomposite was monitored with UV-Vis spectrophotometer. Centrifugation of the resulting nanocomposites mixture at 5000 rpm was done. The supernatant was carefully decanted and disposed of and the residue was left behind. The residue was further scraped and pooled to a clean petri dish. A hot air oven was used to dry the sample at 80 °C and the resulting product was the CNDs-CuO nanocomposite powder that can be further characterized and used.

2.2.6 Characterization of the CNDs, CuO NPs, and CNDs-CuO nanomaterials

It is important to determine some of the properties of the nanomaterials to ensure that they are of quality, pure and certain after they have been synthesized. The formation of the CNDs, CuO NPs and CNDs-CuO nanomaterials were monitored by the use of UV-visible spectrophotometer, Perkin Elmer Lambda 40. The functional groups of the nanomaterials were measured on a Model Nicolet iS10 FT-IR Spectrometer. The shape of both the synthesized of the nanomaterials were traced out using the JOEL JSM-IT71OHR-BECTHAI type scanning electron microscope (SEM). The EDX model of 8100 was used to obtain the elemental composition of the nanomaterials. JEM-ARM200F-G-TEM and Rigaku D/Max-IIIC X-ray diffractometer were used to analyze the size and crystallinity of the nanomaterials.

3.0 RESULTS AND DISCUSSION

3.1 Phytochemical analysis of aqueous extract of RHS

Phytochemical analysis of aqueous extract of RHS in table 1 showed the presence of flavonoids, phenolics, tannin, saponins, alkaloid, terpenoid, glycosides, carbohydrates, reducing sugars, which are characteristic of chemically rich biomass precursor that could be used in the synthesis of nanomaterials. These phytochemicals have a critical role in green synthesis of CuO NPs since they are reducing, stabilizing and capping agents. Specifically, phenolic compounds and flavonoids also enable the process of electron transfer in reduction of metal ions whereas carbohydrates and reducing sugars facilitate carbonization reactions essential in the formation of carbon dot. Later research indicated that biomass carbon dots synthesized using vegetal biomass contain oxygenated surface functionalities in the form of hydroxyl and carboxyl group in biomass-derived carbon dots, which cumulatively are functions of the phytochemicals themselves and are a defining feature of biomass-derived carbon dots (Da'na *et al.,* 2024). Moreover, green synthesis pathways with plant extracts increase the stability and dispersion of nanoparticle as the phytochemicals passivate the surface, thus, enhancing structural integrity and functionality. Therefore, the high phytochemical value of Raphia hookeri supports its appropriateness as a renewable source of compounds to synthesize CuO NPs.

The occurrence of these phytochemicals is directly associated with the electrochemical energy storage capabilities of the synthesized nanocomposite, too. Biomass carbon nanodots have a high surface area, tuneable electronics and admature function groups and guarantee ion adsorption, transfer of charge and electrochemical activity. Phenolics and tannins introduce oxygen-containing groups, which are sources of active redox sites and contribute to pseudo-capacitance and enhance charge storage capacity (Zhang etal., 2020). Also, carbon nanodots are conductive structures that enable the movement of electrons and minimise internal resistance. In combination with CuO NPs that demonstrates inherent faradaic redox characteristics, they show a synergistic effect between electric double-layer capacitance (by carbon nanodots) and pseudo-capacitance (by CuO NPs). This synergy augment power density, cycling stability and capacitance in electrochemical systems (Ren et al., 2024; Sead, 2025). As such, due to the environmental-friendly synthesis supported by the phytochemical composition of Raphia hookeri, it also plays a vital role in enhancing the

electrochemical properties of CuO NPs to be used as energy storage systems (Akpeji *et al.,* 2024c; Wang *et al.,* 2019).

Table 1: Phytochemical analysis of aqueous extract *RHS*

Test performed	Results
Appearance	Liquid
Colour Description	Brown
Flavonoids	+
Steroids	+
Glycoside	+
Reducing sugar	+
Saponin	+
Alkaloids	+
Carbohydrate	+
Phenolic compounds	+
Terpenoids	+
Tannins	+

Keys; (+) Present, (-) Not present

3.2 Characterization of nanomaterials of CNDs, CuO NPs and CNDs-CuO nanomaterials

3.2.1 Optical activity of nanomaterials through UV-Visible spectrophotometer

Figure 1 demonstrates the UV-Visible absorption spectrogram of carbon nanodots (CNDs), CuO nanoparticles, and the hybrid of CND–CuO nanocomposite as a way of understanding the optical activity and electronic structure of each. The peak of absorption at about 280 nm observed with CNDs at that position is typical of π=>pi masses in conjugated sp3 carbon domains and the n=>pi masses in surface functional group areas including C=O which confirms the surface states and quantum confinement effects. In a similar manner, the CuO nanoparticles show a specific absorption peak of about 301 nm, relating to intrinsic band-to-band, and indicates nanoscale size-dependent adjustment of electronic energy levels in nanoscale. The small red-shift and peak broadening of the CND–CuO composite (around 288 nm) demonstrates that there is a high level of interfacial electronic interaction and charge transfer between CNDs and CuO. The spectral changes are commonly observed as signatures of tuning of the band structure and increased electronic interactions in hybrid nanomaterials (Kumar *et al.,* 2024; Prashanth *et al.,* 2025). UV -Vis spectroscopy continues to be one of the primary methods of investigating electronic transitions and approximating optical band gaps in nanostructures (Skoog *et al.,* 2018).

These optical characteristics, as viewed in electrochemical terms of energy storage, translate into enhanced charge storage characteristics. The observed red-shift and increase in the intensity of the absorbance in CND-CuO composite indicate low band-gap energy and high electron mobility, which contribute to high reaction order in electrochemical reactions. Such tunable optical properties of nanomaterials are typically characterized by high conductivity, higher electroactive surfaces, and better ion diffusions, which are critical to high-performance

supercapacitors and battery electrodes (Mohammed *et al.,* 2025; Kumar *et al.,* 2024). CuO provides pseudocapacitative behavior by reversible faradaic reactions, and carbon nanodots efficiently conduct electricity and supply even more active sites. The synergistic interaction leads to enhanced specific capacitance, energy density and cycling stability. Thus, the spectral properties within the UV and Vis spectrum in Figure 1 indicate that the composite indeed formed successfully besides having a high potential in implementing the advanced form of energy storage through electrochemical processes.

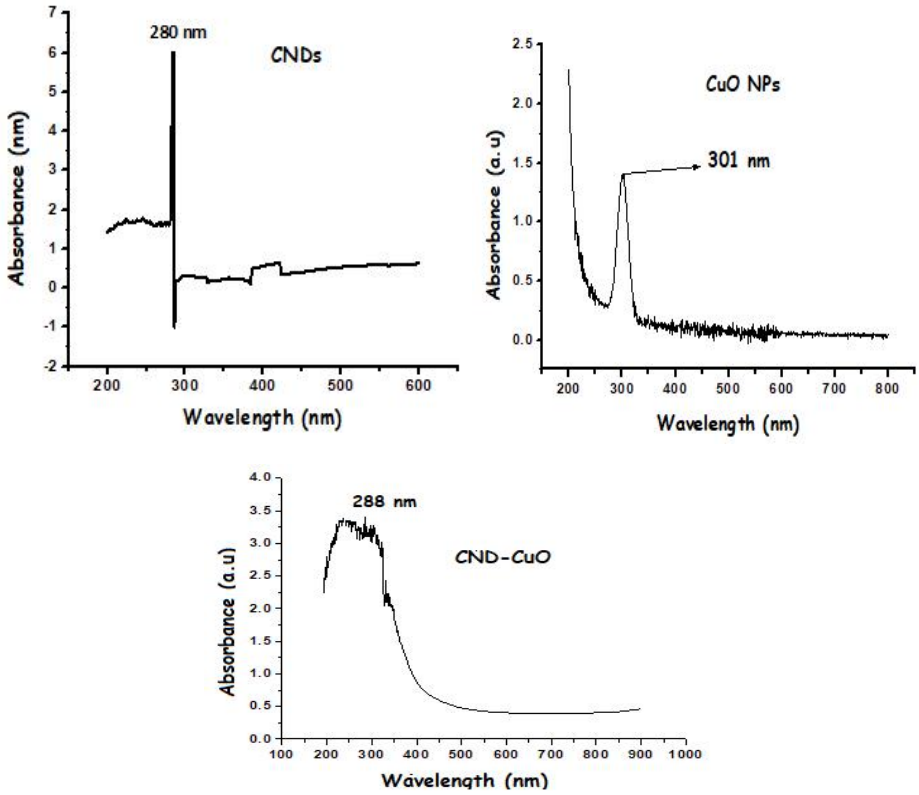

Figure 1: UV-VIS Spectra of nanomaterials

3.2.2 Optical band gap energy of nanomaterials using Tauc's plot

Figure 2 depicts the Tauc's plots to compute the optical band gaps energies of the synthetized nanomaterials where the values are found to be about 2.40 eV of carbon nanodots, (CNDs), 2.29 eV of CuO nanoparticles and 2.32 eV of the CND,CuO nanocomposite. These values of band gap lie in the fine semiconductor realm, which means high absorption in the visible light and high electronic excitation. The small decrease in band gap in the CNDs versus CuO may indicate intrinsic semiconductor characteristics of CuO, whereas the intermediate transmission with the CNDs CND-CuO composite bears evidence of an electronic interaction and the transition of the band structure owing to the formation of heterojunctions. This sort of band gap tuning is highly developed in the nanocomposites, in which charge transfer across interfaces, and defect levels incorporate novel energy states in the band structure, thus lowering the effective energy necessary to

excite electrons (Awad *et al.,* 2025; Mamand *et al.,* 2025). Further, the linear extrapolation doing the Tauc plots is also evidence of direct allowed transitions, common to the metal oxide nanostructures and carbon-based nanomaterials applied in optoelectronic and electrochemical applications.

Electrochemical band gap energies are comparatively low (returning to the 2.29- to 2.40 eV), and this allows the property to promote easier electrical conductivity and rapidities of the electrons relay during the redox reactions. The lower the band gap of the material, the lower the amount of energy is needed to excite the electrons hence, increasing the speed at which charge carriers move and improving kinetics of an electrochemical reaction. This is especially essential in battery electrodes and supercapacitors which rely on fast transfer of electrons and diffusion of ions to define efficiency of performance. More recent discoveries have shown that nanomaterials with a smaller band gap have better electrochemical performance such as a higher specific capacitance, energy density, and enhanced cycling stability, as they have more active sites and defect-induced conductivity (Doroudkhani *et al.,* 2025; Bhatt *et al.,* 2025). Moreover, it was demonstrated that the narrowing of a band gap in hybrid nanocomposites is directly associated with phased ion diffusion and redox activity, resulting in dramatically improved energy storage capacity, with reported capacitance values reported to be over 1000 F/g with optimized systems (Hamza *et al.,* 2026). The band gaps in Figure 2 are thus strong indications that the CND-CuO nanocomposite has improved electrochemical energy storage capacity because of such synergistic electron interactions, conductivity, as well as enhanced transference of charge.

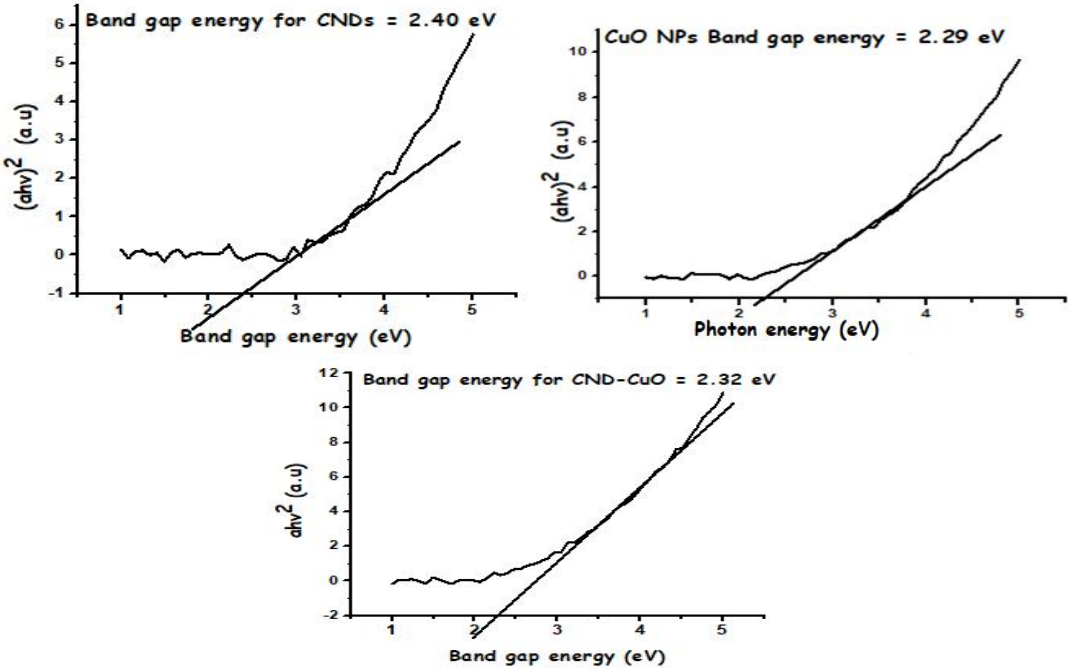

Figure 2: Optical band gap energy of nanomaterials

3.2.3 Morphology of nanomaterials using Scanning Electron Microscope (SEM)

Figure 3 presents the SEM micrographs of the synthesized nanomaterials, highlighting distinct

morphological features for CNDs (A_1), CuO NPs (A_3), and the CND–CuO composite (A_5). The CNDs exhibit agglomerated fine granular structures, typical of carbon nanodots with high surface energy, while the CuO NPs display a porous, sponge-like morphology with interconnected voids that provide a high surface area and abundant electroactive sites. In contrast, the CND–CuO composite shows a more uniform, spherical and well-dispersed nanostructure with reduced aggregation, indicating strong interfacial interaction and successful integration of CNDs within the CuO matrix (Chen *et al.,* 2024). This structural evolution enhances surface accessibility and creates a conductive network that facilitates efficient electron transport. From an electrochemical energy storage perspective, such morphology is highly advantageous, as porous and interconnected structures improve electrolyte penetration and ion diffusion, while the incorporation of conductive carbon nanodots reduces charge transfer resistance and enhances redox kinetics (Breczko *et al.,* 2024). Consequently, the composite is expected to exhibit improved specific capacitance, energy density, and cycling stability compared to the individual components, consistent with reports that morphology-controlled nanocomposites significantly enhance electrochemical performance due to increased active sites and optimized charge transport pathways (Sohouli *et al.,* 2023).

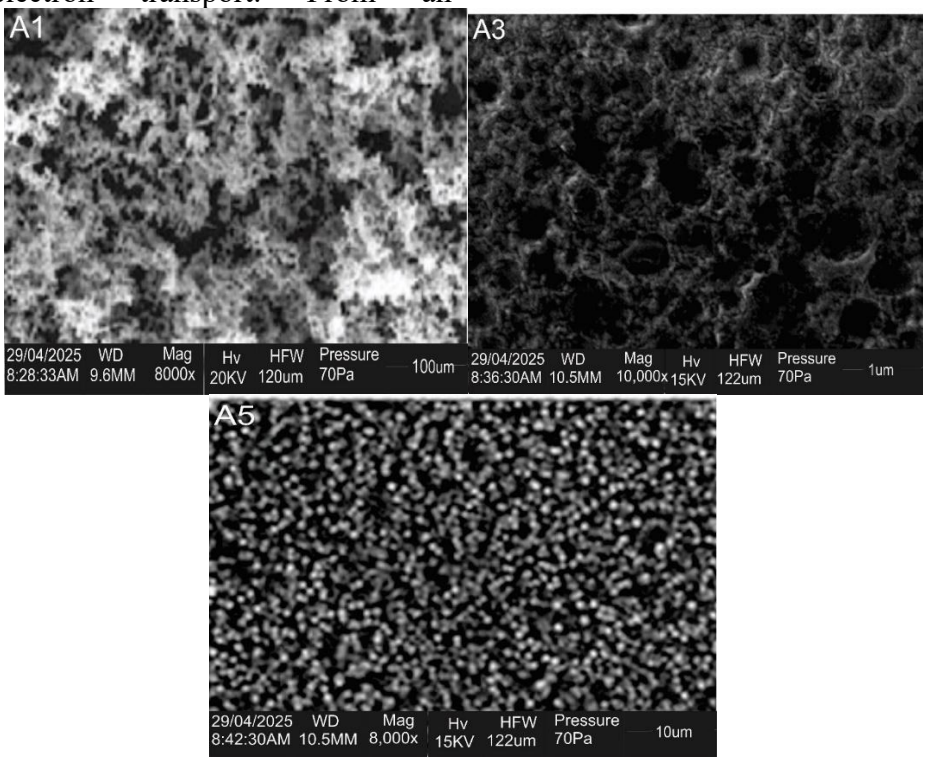

Figure 3: SEM micrographs of nanomaterials (A_1=CNDs, A_3=CuO NPs, A_5= CND-CuO)

3.2.4 Particle size using Transmission Electron Microscope (TEM)

Figure 4 presents the TEM micrographs and particle size distribution of the synthesized nanomaterials, confirming their nanoscale characteristics and uniformity. The CNDs (A1) exhibit well-dispersed spherical particles with an average size of 6.35 nm, while CuO NPs

(A3) show larger particles around 21.0 nm, and the CND–CuO composite (A5) displays an intermediate size of 14.2 nm, indicating successful hybridization and controlled particle growth. The reduction and regulation of particle size in the composite suggest strong interfacial interaction, which limits agglomeration and enhances dispersion. These nanoscale dimensions (<100 nm) are critical for electrochemical applications, as they provide a high surface area, increased active sites, and enhanced surface reactivity due to quantum confinement effects (Mittal *et al.,* 2024; Anney & Biswas, 2026). Smaller particle sizes facilitate faster ion diffusion and improved electron transport, thereby enhancing charge storage efficiency, while the composite structure optimizes conductivity and redox activity by combining CND with CuO. This synergistic effect leads to improved specific capacitance, energy density, and cycling stability, making the material highly suitable for advanced energy storage systems (Mohammed *et al.,* 2025; Prashanth *et al.,* 2025).

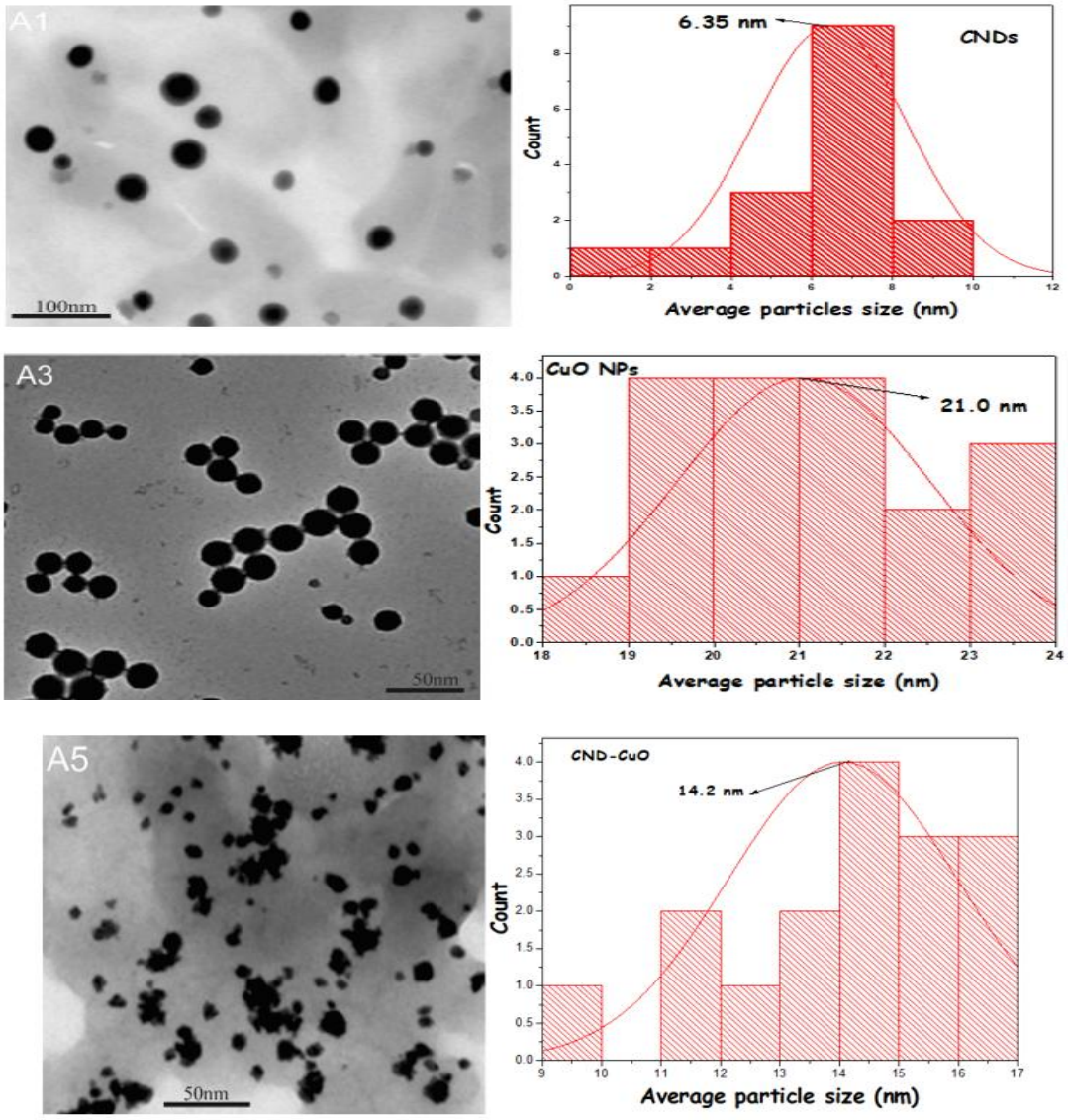

Figure 4: TEM micrographs and average particle size of nanomaterials (A_1= CNDs, A_3= CuO NPs, A_5= CND-CuO)

3.2.7 Elemental constituents using energy dispersive x-ray spectroscopy (EDX)

Figure 4 presents the EDX spectra of the synthesized nanomaterials, confirming their elemental composition and purity. The spectrum for CNDs (A1) shows dominant carbon (90.65 wt%) with a smaller oxygen fraction (9.35 wt%), consistent with CNDs containing oxygenated surface functional groups. The CuO NPs (A3) exhibit strong copper (82.76 wt%) and oxygen (15.24 wt%) peaks with minimal carbon contribution, confirming the successful formation of copper oxide with high phase purity. In the CND–CuO composite (A5), the coexistence of Cu (54.66 wt%), C (40.34 wt%), and O (5.00 wt%) demonstrates effective hybridization and uniform elemental distribution without detectable impurities in ratio 1:1. Furthermore, recent studies on metal oxide–carbon nanocomposites report similar elemental signatures, where the presence of only expected elements confirms phase purity and enhances electrochemical performance by minimizing defect-induced recombination and resistance (Newbury & Ritchie, 2015). Therefore, the EDX results in Figure 4 provide strong evidence of high-quality nanomaterial synthesis, which is crucial for optimizing electron transport, maximizing active sites, and improving overall electrochemical energy storage efficiency.

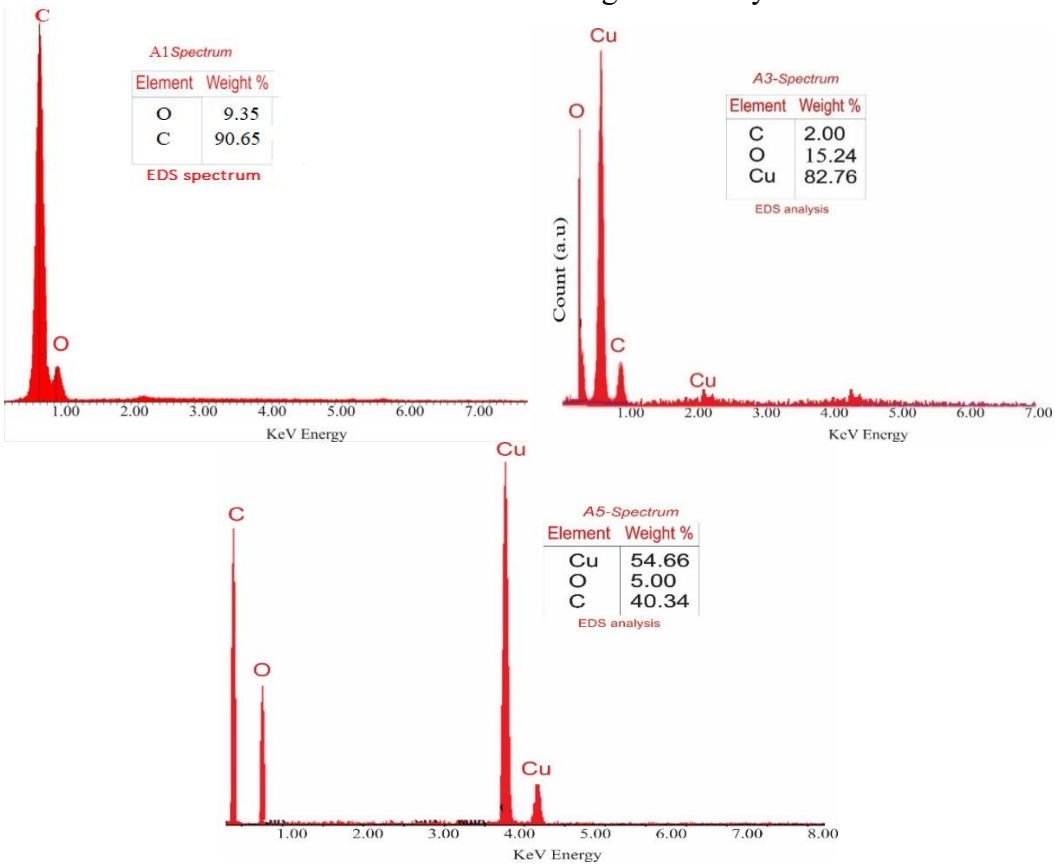

Figure 5: EDX spectra of nanomaterials

3.2.8 Reactive functional groups using FTIR spectrophotometer

Figure 6 presents the FTIR spectra of CNDs, CuO NPs, and the CND–CuO nanocomposite, revealing key functional groups responsible for their chemical structure and interfacial interactions. For CNDs, the broad peak around 3400–3485 cm^{-1} corresponds to O–H stretching vibrations, indicating the presence of hydroxyl groups, while peaks at 2980 cm^{-1} (C–H stretching), 1650 cm^{-1} (C=O stretching), 1350 cm^{-1} (C–H bending), and 1150 cm^{-1} (C–O stretching) confirm the existence of oxygenated functional groups on the carbon surface (Andleeb *et al.,* 2025). These functional groups are typical of carbon nanodots and are crucial for surface passivation, solubility, and electronic properties (Leta *et al.,* 2025). In the CuO NPs, the FTIR spectrum shows similar O–H (3400 cm^{-1}), C–H (2920 cm^{-1}), and C=O (1650 cm^{-1}) bands, along with a distinct peak around 600 cm^{-1} corresponding to Cu–O stretching vibrations, confirming the formation of copper oxide. In the CND–CuO composite, the coexistence of these peaks with slight shifts (e.g., C=O at 1700 cm^{-1} and Cu–O at 400 cm^{-1}) indicates strong interaction between the carbon matrix and CuO, suggesting chemical bonding and successful composite formation.(Pasieczna-Patkowska *et al.,* 2025). The presence of oxygen-containing functional groups (–OH, C=O, C–O) plays a critical role in enhancing electrochemical performance by improving wettability, facilitating electrolyte interaction, and providing active sites for redox reactions. Recent studies highlight that surface-functionalized carbon nanodots and metal oxide nanocomposites exhibit enhanced electrochemical activity due to increased defect sites and improved electron transfer pathways, making them highly suitable for supercapacitor and battery applications (Tavan *et al.,* 2025; Debnath *et al.,* 2025).

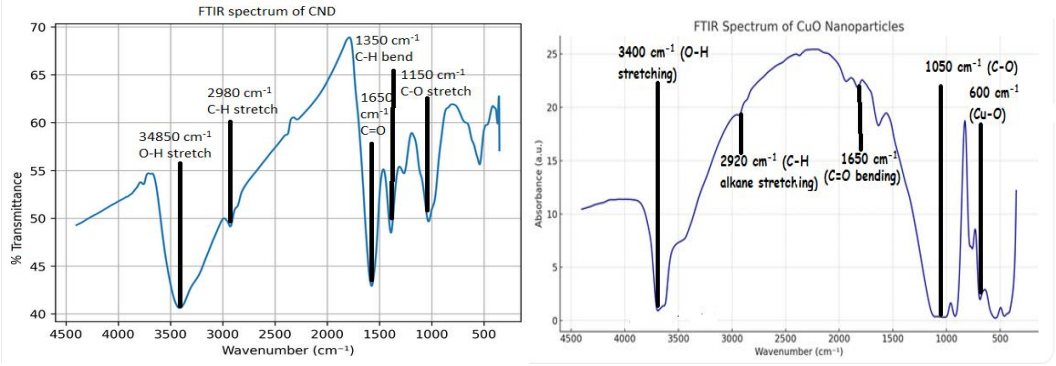

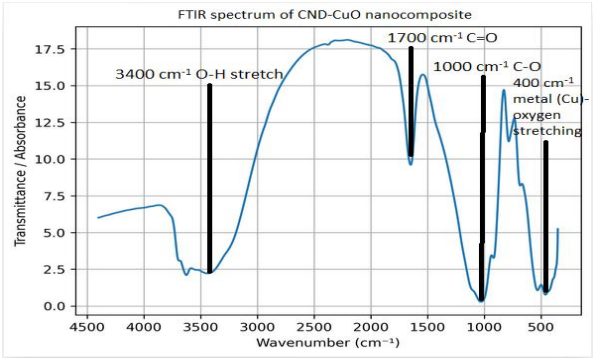

Figure 6: FTIR spectra of nanomaterials

3.2.9 Thermal stability using Thermogravimetry Analysis (TGA)

The heat stability and degradation pattern of CNDs, CuO NPs, and the CND-CuO nanocomposite are shown by providing their thermogravimetric analysis (TGA) curves in Figure 7. The CNDs also exhibit a low-energy loss of the first weight decline at lower temperatures, less than 100 C, due to the evaporation of moisture, and a major degradation (68.6% at 394 C) at the presence of functional groups containing oxygen and carbon structure (Martincic *et al.,* 2024). Likewise, CuO NPs have a high percentage of weight loss (68.5% at 379 C), whereas the CNDCuO composite has a higher temperature stability level with a decomposition temperature peak about 305 C and less loss of mass percentage. The thermal degradation phases observed are typical of a nanocarbon and metal oxide system in which initial weight loss is associated with volatile components, and subsequent weight loss is linked to the structural component and oxidation of the structure (Sabouni et al., 2026). Structurally stable materials at higher temperatures have the capacity to be more electrochemically stable, less degradable, and increase the lifetime of high temperature devices including supercapacitors and batteries. The enhanced thermal characteristics of CNDCuO composite indicate that there exist strong interfacial interactions and high structural robustness this can be translated to resistances to electrochemical degradation and to enhanced charge-discharge cyclic behavior. Recent investigations highlight that carbon based and hybrid nanomaterials are thermally stable and have better electrochemical performance because of their stable active sites, high conductivity, and stability in structural collapse during repeated cycling (Onyancha *et al.,* 2025).

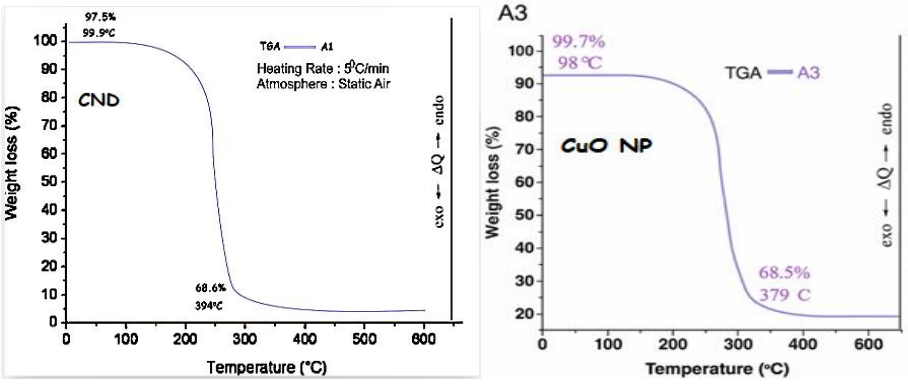

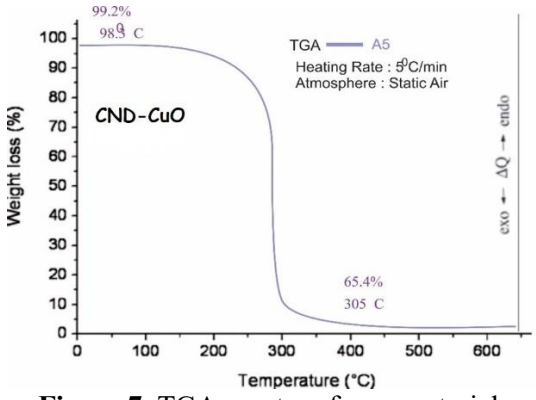

Figure 7: TGA spectra of nanomaterials

3.3 Electrochemical energy storage of nanomaterials

3.3.1 Electrochemical Impedance Spectrophotometer (EIS)

Figure 8 presents the Nyquist plots obtained from electrochemical impedance spectroscopy (EIS) for CNDs, CuO nanoparticles, and the CND–CuO composite, providing insight into their charge transfer resistance and electrochemical kinetics. All samples exhibit semicircular arcs in the high-frequency region, where the diameter corresponds to the charge transfer resistance (Rct). The CND–CuO composite shows the smallest semicircle diameter (lowest Zreal range 5.03–15.43 Ω) compared to CNDs (5.00–17.49 Ω) and CuO (4.98–20.59 Ω), indicating lower charge transfer resistance and improved electrical conductivity. In contrast, CuO nanoparticles display the largest semicircle, reflecting higher resistance to electron transfer. According to EIS theory, a smaller semicircle signifies faster interfacial charge transfer and better electrochemical performance, as impedance spectroscopy effectively deconvolutes resistive and capacitive contributions within electrode materials (Klink *et al.,* 2025; Fang *et al.,* 2025). The reduced impedance observed in the CND–CuO composite confirms enhanced electron transport pathways and improved electrode–electrolyte interaction due to synergistic coupling between conductive carbon nanodots and redox-active CuO. This leads to faster ion diffusion, lower internal resistance, and improved capacitance behavior, which are critical for high-performance supercapacitors and batteries. Recent studies emphasize that nanocomposites with reduced charge transfer resistance exhibit superior rate capability, energy density, and cycling stability because EIS directly reflects kinetic limitations in electrochemical systems (Bakenhaster *et al.,* 2025; Silva *et al*., 2025; Zhang *et al.,* 2025). Therefore, the EIS results clearly demonstrate that the CND–CuO composite possesses the best electrochemical performance among the samples, owing to its minimized resistance and enhanced charge transport properties.

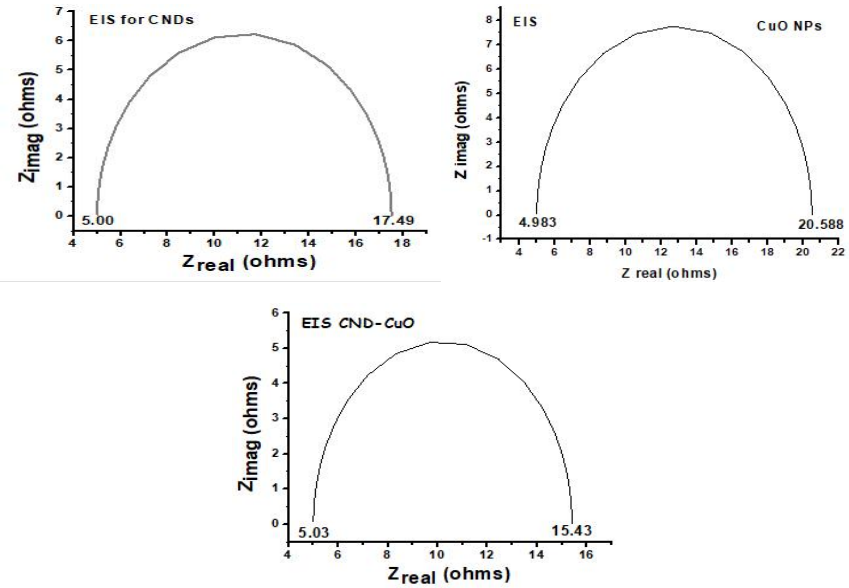

Figure 8: EIS of nanomaterials

3.3.2 Cyclic Voltammetry (CV)

Figure 8 presents the cyclic voltammetry (CV) curves of CNDs, CuO NPs, and the CND–CuO composite, revealing distinct redox behavior and charge storage characteristics. The CNDs exhibit relatively low current response with broader peaks, indicating limited electrochemical activity dominated by electric double-layer capacitance. In contrast, CuO nanoparticles display more defined anodic and cathodic peaks, reflecting faradaic redox reactions typical of pseudocapacitive materials. Notably, the CND–CuO composite shows the highest current response and more pronounced redox peaks, indicating enhanced electrochemical activity, improved reversibility, and faster charge transfer kinetics. The increased peak current and reduced peak separation in the composite suggest lower internal resistance and better electron/ion transport, confirming synergistic interaction between conductive carbon nanodots and redox-active CuO. Cyclic voltammetry is widely used to evaluate energy storage performance, where higher current response and well-defined peaks correspond to improved capacitance and charge storage efficiency (Rahimkhoei *et al.,* 2025). Furthermore, recent studies highlight that hybrid nanocomposites enhance electrochemical performance by combining electric double-layer capacitance and pseudocapacitance, leading to superior energy density and rate capability (Farsi *et al*., 2025; Prashanth *et al*., 2025). The improved behavior of the composite is attributed to increased active sites, enhanced conductivity, and efficient ion diffusion pathways, which are critical for high-performance supercapacitors and batteries (Gangipamula *et al*., 2025; Mohammed *et al.,* 2025). Therefore, the CV results clearly demonstrate that the CND–CuO composite possesses the best electrochemical energy storage potential among the samples due to its optimized charge storage mechanism and enhanced electrochemical kinetics.

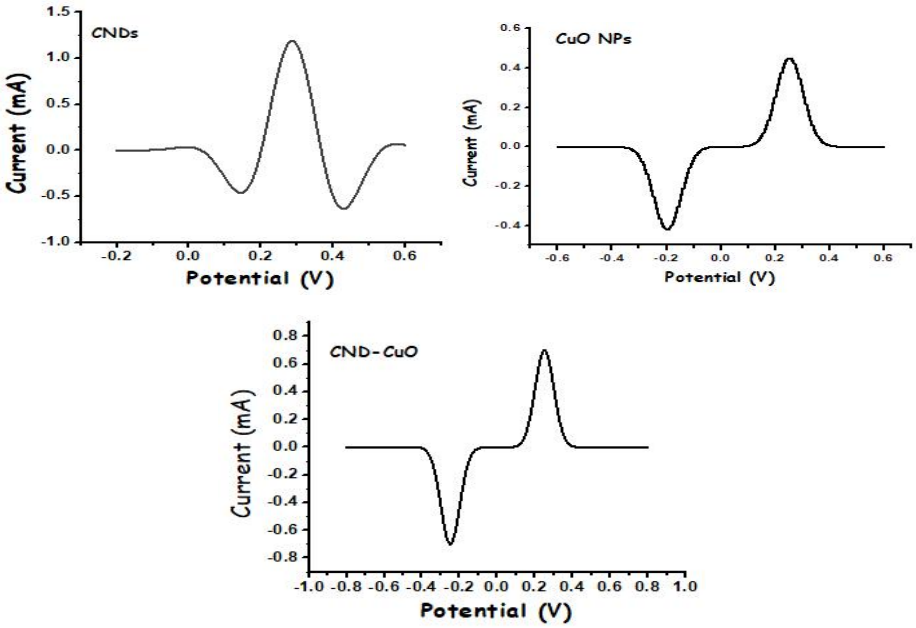

Figure 9: Cyclic voltammogram of nanomaterials

4.0 CONCLUSION

This study successfully demonstrates the development of a sustainable carbon nanodot–copper oxide (CND–CuO) nanocomposite derived from *Raphia hookeri* seed (RHS) biomass and its applicability for electrochemical energy storage. The phytochemical richness of RHS (flavonoids, phenolics, tannins, and other bioactive compounds) provided an effective green route for nanoparticle synthesis and stabilization. Comprehensive characterization confirmed the successful formation of the nanocomposite: UV–Vis and band gap analysis revealed tunable electronic properties; FTIR verified the presence of functional groups and strong interfacial interactions; SEM and TEM showed nanoscale, well-dispersed morphology with optimized particle size; and EDX confirmed high purity and appropriate elemental composition. Electrochemical evaluations clearly established the superiority of the CND–CuO composite over the individual components. The composite exhibited reduced charge transfer resistance in EIS analysis, enhanced redox activity and higher current response in cyclic voltammetry, and improved structural integration. Although CuO nanoparticles demonstrated the highest thermal stability, the composite provided the best balance between conductivity, electrochemical activity, and structural performance. This synergistic effect arises from the combination of conductive carbon nanodots and redox-active CuO, which enhances electron transport, increases active sites, and improves ion diffusion pathways. In conclusion, the CND–CuO nanocomposite synthesized from RHS biomass is a promising, low-cost, and environmentally friendly electrode material with significant potential for high-performance electrochemical energy storage systems, including supercapacitors and batteries.

5.0 Declaration of Competing Interest

The authors declare that they have no known competing interests.

6.0 Acknowledgments

The authors acknowledge the support of the Tertiary Education Trust Fund (TETFund). The authors also appreciate the technical assistance provided by staff of the Department of Chemistry, University of Benin and Department of Science Laboratory Technology,

Federal University of Petroleum Resources, Effurun.

REFERENCES

Akpeji, B. H., Akusu, P. O., Emegha, M. C., Onyenue, E. E., & Elemike, E. E. (2024b). Synthesis and characterization of carbon dot from plastic waste for remediation of Fe^{3+} in wastewater. *International Journal of Research and Innovation in Applied Science*, 9(6), 14–18. https://doi.org/10.51584/IJRIAS.2024.906002.

Akpeji, B. H., Emegha, M. C., Onyenue, E. E., Meshack, O. Q., & Elemike, E. E. (2024a). Synthesis and characterization of nanoparticles of ZnO, carbon dot and ZnO–carbon dot nanocomposite from groundnut shell wastes. *Journal of Applied Science and Environmental Management*, 28(6), 1771–1780. https://doi.org/10.4314/jasem.v28i6.16.

Akpeji, B. H., Korede, T. B., & Adedokun, J. (2024d). Removal of Mn (II) ions from aqueous solution using silver and titanium dioxide nanoparticles derived from bacterial pigment: Experimental characterization and optimization. *Advances in Industrial Engineering and Management (AIEM)*, 13(2), 154–165. https://doi.org/10.7508/alem.02.2024.154.165.

Akpeji, B. H., Laric, B., Igbuku, U. A., Tesi, G. O., Elemike, E. E., & Akusu, P. O. (2024c). Synthesis and characterization of MnO_2 nanoparticles mediated by RHS. *Journal of the Nigerian Society of Physical Sciences*, 6, 2203. https://doi.org/10.46481/jnsps.2024.2203.

Akpeji, B. H., Okhuarobo, L. O., Akakabota, A. O., Okologume, J. O., & Osio, O. L. (2025). Conversion of plastic polymeric wastes into carbon dots: A sustainable approach. *Anchor University Journal of Science and Technology*, 6(2), 187–192. https://doi.org/10.4314/aujst.v6i2.2.

Akpeji, B. H., Singh, V. (2026). Synthesis and characterization of magnesium oxide nanoparticles (MgO NPs) derived from RHSs (RHS) and evaluation of their nano-pharmacokinetic properties. *Discover Chemistry*, 3, 129. https://doi.org/10.1007/s44371-026-00597-6.

Andleeb, N., Ali, S., Khan, M. A., & Ahmed, S. (2025). Carbon quantum dots as versatile nanomaterials for improving plant stress tolerance and productivity. *Planta*, 261(2), 45. https://doi.org/10.1007/s00425-025-04758-2 (doi.org in Bing)

Anney, A., & Biswas, S. (2026). Nanomaterials in energy storage and sensing: A comprehensive review. *World Journal of Nano Science and Engineering*, 16(1), 1–21. https://doi.org/10.4236/wjnse.2026.161001.

Arora, G., Sabran, N. S., Ng, C. Y., & Low, F. W. (2024). Applications of carbon quantum dots in electrochemical energy storage devices. *Heliyon*, 10(18), e35543. https://doi.org/10.1016/j.heliyon.2024.e35543.

Awad, M. A., El-Sayed, A. M., Hassan, M. A., & Abdelrahman, E. A. (2025). Optical and structural characteristics of La_2O_3–ZnO nanoparticles for advanced applications. *Results in Engineering*, 21, 101234. https://doi.org/10.1016/j.rineng.2025.101234.

Bakenhaster, S. T., Johnson, M. R., & Lee, C. H. (2025). Electrochemical impedance spectroscopy and battery systems: Recent advances and future perspectives. *Journal of Applied Electrochemistry*. https://doi.org/10.1007/s10800-025-02273-6.

Bhatt, M., Gautam, K., Verma, A. K., & Sinha, A. K. (2025). Structural, optical, surface chemical, and electrochemical characterization of Aloe vera-assisted

ZnO nanostructures for supercapattery applications. *Materials Advances*, 6(16), 5618–5632. https://doi.org/10.1039/D5MA00556F

Breczko, J., Nowak, P., & Lisowska-Oleksiak, A. (2024). Zero-dimensional carbon nanomaterials for electrochemical energy storage applications. *ChemElectroChem*, 11(3), e202300752. https://doi.org/10.1002/celc.202300752.

Chakrabarti, A., Das, S., & Roy, P. (2025). Recent advancement of quantum dot-based nanocomposites for energy storage applications. *Energies*, 18(3), 630. https://doi.org/10.3390/en18030630.

Chen, T. W., Zhang, Y., & Liu, H. (2024). Electrochemical energy storage applications of carbon-based nanocomposites: Morphology–performance relationship. *Materials Today Energy*, 37, 101456. https://doi.org/10.1016/j.mtener.2024.101456.

Chowdhury, Z., Rahman, M., & Islam, M. (2024). Optical characterization of nanofluids using UV–Vis spectroscopy for stability assessment. *Results in Engineering*, 21, 101745. https://doi.org/10.1016/j.rineng.2024.101745.

Da'na, E., Parveen, N., Taha, A., & El-Aassar, M. R. (2024). CuO/NiO nanocomposite prepared with Saussurea costus extract for supercapacitor energy storage application. *Nanocomposites*, 10(1), 283–297. https://doi.org/10.1080/20550324.2024.2363733.

Debnath, R., Ghosh, S., & Das, P. (2025). Carbon nanodots-based polymer nanocomposites: Recent advances and applications. *Polymers*, 17(3), 365. https://doi.org/10.3390/polym17030365.

Doroudkhani, Z. S., Mazloom, J., & Ghaziani, M. M. (2025). Optical and electrochemical performance of electrospun NiO–Mn_3O_4 nanocomposites for energy storage applications. *Scientific Reports*, 15, 11436. https://doi.org/10.1038/s41598-025-96008-4.

Fang, R., Zhao, X., & Liu, Y. (2025). Mechano-electrochemical impedance spectroscopy for advanced battery diagnostics. *Joule*. https://doi.org/10.1016/j.joule.2025.03.012.

Gangipamula, V., Subhani, K., Mahon, P. J., & Salim, N. (2025). Nanomaterial functionalized carbon fiber-reinforced composites with energy storage capabilities. *Nanomaterials*, 15(17), 1325. https://doi.org/10.3390/nano15171325.

Gusain, M., Kumar, N., & Singh, R. (2025). Advanced carbon nanomaterials for high-performance energy storage systems. *Materials Today Energy*. https://doi.org/10.1016/j.mtener.2025.101456.

Haghjou, F., Rahimi, A., & Karimi, M. (2025). Synergistic effects of CuO-based nanocomposites with carbon materials for electrochemical performance enhancement. *Journal of Materials Science*. https://doi.org/10.1007/s10853-025-09876-2.

Hamza, A. M., Ali, S. H., Ibrahim, Y. A., & Khalil, M. A. (2026). Tailored electrochemical and energy storage properties of plasma-modified NiO-based nanocomposites. *Applied Physics A*, 132(2), 145. https://doi.org/10.1007/s00339-026-09494-2.

Huang, X., Li, Y., Zhang, L., Wang, H., & Chen, Z. (2025). Carbon dots for advanced electrochemical energy storage: Mechanisms, design strategies, and applications. *Nano Energy*, 118, 108456. https://doi.org/10.1016/j.nanoen.2025.108456.

Ibiyemi, A. O., Adeyemi, T. O., Ogunleye, A. A., & Bello, S. A. (2025). Influence of pH on optical and structural properties of Nb-doped V_2O_5 nanoparticles for energy applications. *African Scientific Reports*, 4(1), 310. https://doi.org/10.46481/asr.2025.310

Jin, Y. (2024). Advances in carbon dot-based nanomaterials for energy storage applications. *Journal of Energy Storage*, 78, 107235. https://doi.org/10.1016/j.est.2024.107235

Klink, R., Müller, T., & Schmidt, A. (2025). Electrochemical impedance spectroscopy for lithium-ion batteries: Measurement and analysis. *Current Opinion in Electrochemistry*. https://doi.org/10.1016/j.coelec.2025.101768

Kumar, A., Singh, R., & Verma, P. (2024). Hybrid nanomaterials for high-performance supercapacitor applications. *Colloids and Surfaces A: Physicochemical and Engineering Aspects*, 678, 132456. https://doi.org/10.1016/j.colsurfa.2023.132456.

Leta, T. B., Gemechu, F. K., & Tadesse, A. (2025). Carbon dot nanoparticles synthesized from horticultural waste for sustainable applications. *Plants*, 14(16), 2523. https://doi.org/10.3390/plants14162523.

Mametja, L. D., Mubiayi, K. P., & Moloto, M. J. (2026). Carbon dot–metal oxide nanocomposites for electrochemical energy storage applications: A review. *Materials Advances*, 7(3), 1456–1472. https://doi.org/10.1039/D5MA00927H.

Mittal, A., Sharma, R., & Gupta, P. (2024). Characterization of advanced nanomaterials for energy storage applications. *E3S Web of Conferences*, 67, 07012.

Mohammed, A. S., Ibrahim, H. G., Abdullahi, M. B., & Sani, U. (2025). Enhanced electrochemical performance of carbon dot–CuO nanocomposites for supercapacitor applications. *Journal of Materials Science: Materials in Electronics*, 36(5), 4123–4135. https://doi.org/10.1007/s10854-025-11892-3.

Newbury, D. E., & Ritchie, N. W. M. (2015). Is scanning electron microscopy/energy dispersive X-ray spectrometry (SEM/EDS) quantitative? *Scanning*, 37(3), 141–168. https://doi.org/10.1002/sca.21167.

Okorhi, F. B., & Akpeji, B. H. (2024). Carbon dot soil enhancement: Creating a new era of environmentally conscious and climate-adaptive agriculture. *Global Research in Environment and Sustainability*, 3(1), 17–30.

Pasieczna-Patkowska, S., Nowicka, A., & Kowalski, K. (2025). Application of Fourier transform infrared (FTIR) spectroscopy in nanoparticle characterization: A review. *Materials*, 18(3), 789. https://doi.org/10.3390/ma18030789.

Prashanth, G. K., Rao, S., Lalithamba, H. S., Bhagya, N. P., Swamy, M. M., & Yogananda, H. S. (2025). Smart nanomaterials for semiconductor applications: Advances in energy storage and biosensing technologies. *Next Materials*, 4(1), 100964. https://doi.org/10.1016/j.nxmate.2025.100964.

Rahimkhoei, V., Ahmadi, M., & Karimi, A. (2025). Exploration of electrochemical energy storage potential of nanomaterials using cyclic voltammetry. *Arabian Journal of Chemistry*. https://doi.org/10.1007/s13201-025-02470-w.

Ren, J., Liu, Y., Zhao, X., & Wang, Q. (2026). Sustainable synthesis of biomass-derived carbon dots for high-performance energy storage devices. *ACS Sustainable*

Chemistry & Engineering, 14(2), 2150–2162. https://doi.org/10.1021/acssuschemeng.5c00179.

Sead, A. M., Rahman, M. M., Hossain, M. S., & Karim, M. R. (2025). Heteroatom-doped carbon dots for high-performance supercapacitors: Recent advances and future prospects. *Journal of Nanoscience and Nanotechnology*, 25(4), 1452–1465. https://doi.org/10.1166/jnn.2025.25052

Sikiru, S. A., Bello, O. S., & Adeyemi, O. T. (2023). Advances and prospects of carbon quantum dots synthesis for energy storage applications. *Journal of Energy Storage*, 60, 106556. https://doi.org/10.1016/j.est.2022.106556.

Silva, L. M., Santos, P. R., & Costa, J. F. (2025). Electrochemical impedance spectroscopy as a tool to monitor interfacial processes in electrochemical systems. *Electrochimica Acta*. https://doi.org/10.1016/j.electacta.2025.142345.

Skoog, D. A., Holler, F. J., & Crouch, S. R. (2018). *Principles of instrumental analysis* (7th ed.). Cengage Learning.

Sohouli, E., Shabani-Nooshabadi, M., & Ganjali, M. R. (2023). High-performance CuO/carbon nanocomposite electrodes for supercapacitor applications. *Scientific Reports*, 13, 43430. https://doi.org/10.1038/s41598-023-43430-1.

Surana, K. (2025). Green synthesis of carbon nanodots from biomass for energy and environmental applications. *Renewable & Sustainable Energy Reviews*, 189, 113980. https://doi.org/10.1016/j.rser.2025.113980

Tavan, M., Yousefian, Z., Bakhtiar, Z., Rahmandoust, M., & Mirjalili, M. H. (2025). Carbon quantum dots: Multifunctional fluorescent nanomaterials for sustainable advances. *Industrial Crops and Products*, 231, 121207. https://doi.org/10.1016/j.indcrop.2025.121207.

Vitha, M. F. (2020). *Spectroscopy: Principles and instrumentation* (2nd ed.). Wiley.

Wang, Y., Hu, A., & Chen, X. (2019). Green synthesis of metal oxide nanoparticles using plant extracts and their applications. *Materials Letters*, 236, 68–71. https://doi.org/10.1016/j.matlet.2018.10.089

Zhang, H., Wang, Y., & Li, Q. (2025). Electrochemical impedance spectroscopy-based nanomaterial design for high-performance energy storage systems. *Biosensors*, 15(7), 443. https://doi.org/10.3390/bios15070443.

Zhang, J., Yu, S. H., & Wang, X. (2020). Carbon-based nanomaterials for advanced energy storage. *Advanced Energy Materials*, 10(14), 1901973. https://doi.org/10.1002/aenm.201901973.

Zhang, Y., Li, X., & Chen, H. (2023). Metal oxide–carbon nanocomposites for electrochemical energy storage applications. *Journal of Energy Storage*, 58, 106344. https://doi.org/10.1016/j.est.2022.106344.

Zhao, J., Wang, Q., & Liu, Y. (2021). Review on supercapacitors: Technologies and performance evaluation. *Journal of Energy Chemistry*, 59, 276–291. https://doi.org/10.1016/j.jechem.2020.11.013.